Pt-Decorated g-C₃N₄/TiO₂ Nanotube Arrays with Enhanced Visible-Light Photocatalytic Activity for H₂ Evolution

Zhi-Da Gao+,[a] Yong-Fang Qu+,[a] Xuemei Zhou+,[b] Lei Wang+,[b] Yan-Yan Song+,*[a] and Patrik Schmuki+*[b, c]

Aligned TiO_2 nanotube layers (TiNTs) grown by self-organizing anodization of a Ti-substrate in a fluoride-based electrolyte were decorated with graphitic-phase C_3N_4 (g-C_3N_4) via a facile chemical vapor deposition approach. In comparison with classical TiO_2 nanotubes (anatase), the g-C_3N_4/TiNTs show an onset of the photocurrent at 2.4 eV (vs. 3.2 eV for anatase) with a considerably high photocurrent magnitude in the visible range. After further decoration with Pt nanoparticles, we obtained a visible-light responsive platform that showed, compared with g-C_3N_4-free TiNTs, a strong enhancement for photoelectrochemical and bias-free H_2 evolution (15.62 μLh^{-1} cm^{-2}), which was almost a 98-fold increase in the H_2 production rate of TiNTs (0.16 μLh^{-1} cm^{-2}). In a wider context, the g-C_3N_4-combined 3D nanoporous/nanotubular structure thus provides a platform with significant visible-light response in photocatalytic applications.

Titanium dioxide (TiO_2) is the most studied photocatalyst in contemporary science and technology,[1] namely due to its use in decomposing organic pollutants in the environment (e.g. in self-cleaning coatings on buildings) and also due to its antimicrobial properties.[2–5] For photocatalysis, TiO_2 is irradiated with light of an energy equal to or higher than its band-gap energy (3.0–3.2 eV), and electron-hole pairs are generated in the conduction and valance band of TiO_2, respectively. The holes emitted from the valance band and electrons from the conduction band can be used for phtotocatalytic reactions, for example, to oxidize an organic compound or to "split" water into H_2 and O_2.[6,7] In order to optimize the performance of photocatalysts as suspension or photoelectrodes, a large number of TiO_2 morphologies have been explored. One of the most investigated morphologies are aligned TiO_2 nanotube layers (TiNTs). These TiNTs can be formed by self-ordering electrochemical anodization of Ti. The wide research interest in these materials is due to a unique combination of their geometry and reactivity.[8–10] Particularly, photoconversion efficiencies of nanotubular arrays of TiO_2 were reported to be very high due to a high charge transfer rate and orthogonal carrier separation.[11,12] An intrinsic drawback of TiO_2 is, however, its large band-gap (3.2 eV for anatase-type and 3.0 eV for rutile-type) that makes it active only in the UV spectral range ($\lambda < 387$ nm) which accounts for less than 5% of solar light. Therefore, numerous approaches to achieve a visible response by band-gap engineering (doping)[4,13] or sensitization (e.g., by dyes[14] with other semiconductors[15–19] or other photoactive compounds[20–24]) have been reported.

Recently, graphitic carbon nitride (g-C_3N_4) has attracted considerable attention as a potential visible-light photocatalyst owing to its visible-light band-gap at 2.69 eV and its comparably high stability.[25–28] However, the photocatalytic performance of g-C_3N_4 is limited by the low quantum efficiency for the pristine semiconductor. To resolve this problem, many attempts have been carried out to improve the photocatalytic performance of g-C_3N_4, by for example, nonmetal doping,[29–32] preparation of nano/porous C_3N_4,[33,34] and formation of heterojunction between C_3N_4 and other materials.[35–40] The highest occupied molecular orbital (HOMO) of the g-C_3N_4 is located more negative than the conduction band (CB) of several common wide band-gap semiconductor photocatalysts such as TiO_2, ZnO, and $BiPO_4$. Thus, by constructing heterojunctions with g-C_3N_4, these wide band-gap semiconductors can be sensitized by g-C_3N_4, and a visible-light response can be obtained.

In the present work, we explore the feasibility to decorate and activate TiO_2 nanotube arrays by graphitic carbon nitride (g-C_3N_4) and explore them for visible-light photocatalytic H_2 generation. We chose melamine as the precursor for a direct synthesis of g-C_3N_4 and TiO_2 nanotube (g-C_3N_4/TiNTs) decoration using a one-step chemical vapor deposition (CVD) technique. The g-C_3N_4 loaded anatase TiO_2 nanotubes were then investigated for photocatalytic H_2 evolution under solar illumination conditions, in a photoelectrochemical configuration as well as under open-circuit potential (OCP) conditions. We show that a considerable enhancement for H_2 evolution under both conditions can be obtained.

Figure 1A,B show scanning electron microscopy (SEM) images of the top view and the cross-sectional view of the

[a] Prof. Dr. Z.-D. Gao,+ Y.-F. Qu,+ Prof. Dr. Y.-Y. Song+
College of Sciences, Northeastern University, Shenyang 110004 (P. R. China)
E-mail: yysong@mail.neu.edu.cn

[b] X. Zhou,+ Dr. L. Wang,+ Prof. Dr. P. Schmuki+
Department of Materials Science and Engineering, WW4-LKO
University of Erlangen–Nuremberg
Martensstrasse 7, Erlangen 91058 (Germany)
E-mail: schmuki@ww.uni-erlangen.de

[c] Prof. Dr. P. Schmuki+
Department of Chemistry, Faculty of Science
King Abdulaziz University, Jeddah 21569 (Saudi Arabia)

[+] Z.-D. G. and P. S. conducted the research and discussed the results. Y.-F. Q. prepared the samples, X. Z. carried out the H_2 evolution test, and L. W. carried out the photoelectrochemical test. Y.-Y. S. carried out the electrochemical experiments, Y.-F. Q. and X. Z. carried out the materials characterizations. Z.-D. G. and Y.-Y. S. drafted the paper. All of the authors reviewed the manuscript and participated in discussions on the results of this research.

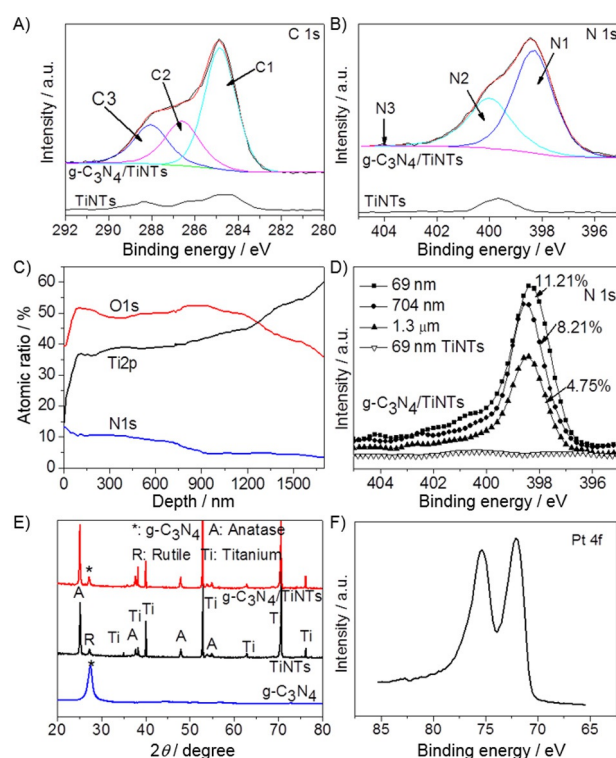Supporting information for this article is available on the WWW under http://dx.doi.org/10.1002/open.201500219.
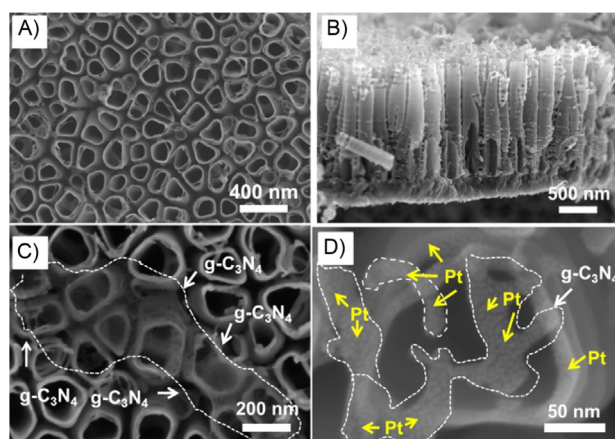
Figure 1. SEM images: A) top view and B) cross-sectional view of TiO$_2$ nano-tube arrays, C) top view of TiO$_2$ nanotube arrays after modification with g-C$_3$N$_4$ by using 15 mg melamine as a precursor, and D) magnified top view of g-C$_3$N$_4$/TiO$_2$ nanotube arrays after further decoration with Pt nanoparticles.


Figure 2. XPS core-level spectra of TiO$_2$ nanotube arrays before and after being modified with g-C$_3$N$_4$ by using 15 mg melamine as a precursor for A) C 1s and B) N 1s. C) XPS depth-profiling spectra of O 1s, N 1s, and Ti 2p peaks for g-C3N4-modified TiNTs, and D) the corresponding core-level spectra of N 1s for g-C3N4/TiNT and TiNT samples. E) XRD patterns of TiO$_2$ nanotube arrays annealed at 550 °C; g-C3N4 and g-C3N4-modified TiO$_2$ nanotube arrays prepared at 550 °C. (F) The XPS score-level spectra for Pt 4f of the Pt/g-C$_3$N$_4$/TiNT sample.

TiO$_2$ nanotube layer before loading with g-C$_3$N$_4$. The tubes have an average diameter of 150 nm, and the layer has a thickness of approximately 1.5 µm. Figure 1 C and Figure S1 A (in the Supporting Information) show the nanotubes after loading with g-C$_3$N$_4$ by using 15 mg melamine as a precursor. Compared with the neat nanotubes, distinct patches of g-C$_3$N$_4$ nanofilm can be seen on the tube wall and entrance (Figure 1 C)—this appearance of g-C$_3$N$_4$ is well in line with literature of g-C$_3$N$_4$ deposition on other substrates.[40] It should be noted that using our deposition process, a loading of the nanotubes from 15 mg melamine precursor represents an optimized treatment. In a set of preliminary experiments, a number of modification conditions (i.e. annealing temperature, temperature rise rate, Ar flow speed) were explored. As shown in Figure S2 in the Supporting Information, with further increase in the amount of precursor, large agglomerates of g-C$_3$N$_4$ were observed on the surface of the tubes which can block the tube mouths. Figure 1 D and Figure S1 B in the Supporting Information show the g-C$_3$N$_4$/TiNTs after depositing Pt by sputtering—the particles have a size of approximately 2 nm and preferably are loaded at the tube mouth.

The successful decoration with g-C$_3$N$_4$ was further verified by X-ray photoelectron spectroscopy (XPS) analysis. The XPS survey spectra in Figure S3 (Supporting Information) characterize TiNT samples before and after the g-C$_3$N$_4$ decoration. Figure 2 A,B shows the C 1s and N 1s spectra for g-C$_3$N$_4$/TiNTs, and the spectra of bare TiNTs are also included as reference. The C 1s spectra of g-C$_3$N$_4$/TiNTs in Figure 2 A exhibit three peaks located at 284.8, 286.6, and 288.0 eV. The peak at 284.6 eV (C1) is typically ascribed to sp^2 C=C bonds, the peak at 286.6 eV (C2) can be assigned to the sp^2-hybridized carbon atoms bonded to three nitrogen atoms in the g-C$_3$N$_4$ layer, and the peak at 288.0 eV (C3) can be attributed to the sp^2 carbon atoms in the aromatic ring attached to the —NH$_2$ group.[41] In Figure 2 B, the corresponding high-resolution N 1s spectrum of the g-C$_3$N$_4$/TiNTs can be fitted by three peaks centered at 398.3 (N1), 400.0 (N2), and 404.0 eV (N3), which correspond to sp^2-bonded

N involved in the triazine rings (C—N=C), the bridging N atoms in N—(C)$_3$, and the amino functions carrying hydrogen (N—H),[42] correspondingly. For the reference tubes, the appearance of the N 1s peak likely originates from the N-containing electrolyte in the anodization process and N$_2$ absorbance from environment, which only exists on the top of tubes. To study the contribution of g-C$_3$N$_4$ on the nanotubes, the higher energy peak of C 1s, O 1s, and Ti 2p is considered for sputtering profiles. As illustrated in Figure 2 C,D, a very clear indication of sputter removal of a g-C$_3$N$_4$ and TiO$_2$ tube layer is obtained. The N 1s signal (398.3 eV) is lost with the O 1s (532.2 eV). In comparison with reference tubes without C$_3$N$_4$ coating, the N 1s peak is visible even at ~1.3 µm, which is very close to the bottom of the tubes. The successful decoration with g-C$_3$N$_4$ was also analyzed by X-ray diffraction (XRD), as shown in Figure 2 E. For g-C$_3$N$_4$, a typical peak was found at 27.6°, which corresponds to the characteristic interplanar stacking peak of aromatic systems in the (002) diffraction plane.[25] From g-C$_3$N$_4$-loaded TiO$_2$ nanotubes, only the diffraction peaks of the anatase phase were observed from the g-C$_3$N$_4$/TiNTs XRD pattern due to comparably small amounts and lower crystallinity of C$_3$N$_4$.[40] However, the peak at 27.6° present in the spectrum of g-C$_3$N$_4$/TiNTs could also be assigned to the presence of some rutile TiO$_2$. Finally, the successful loading of Pt was also confirmed by XPS (Figure 2 F).
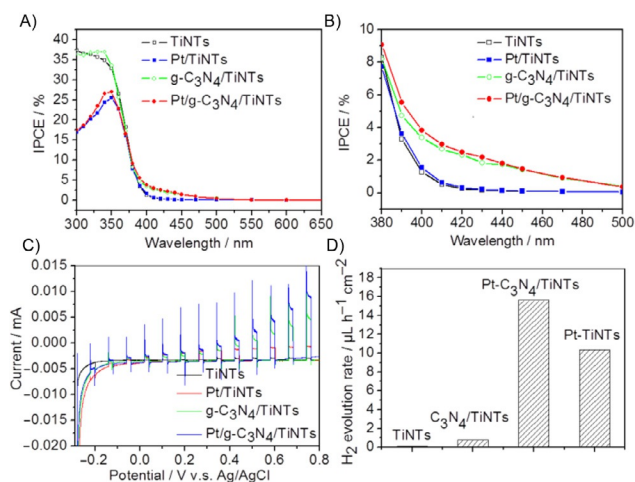
Figure 3. A) IPCE spectra and B) enlarged IPCE spectra at a bias of 0.5 V in 0.1 M Na_2SO_4, C) water splitting performances in a 0.1 M Na_2SO_4 under AM 1.5 with a 400 nm filter, and D) photocatalytic bias-free H_2 production in 20 vol % EtOH in H_2O under AM 1.5 for g-C_3N_4/TiNT, Pt/g-C_3N_4/TiNT, Pt-TiNT, and TiNT samples.

To evaluate the photoelectrochemical properties of the different stages of g-C_3N_4-loaded TiO_2 nanotubes, incident photon-to-current conversion efficiency (IPCE) spectra were measured and compared with neat anatase TiO_2 (Figure 3 A,B). In the visible-light region, g-C_3N_4/TiNTs exhibited a considerably enhanced IPCE with an onset at about 2.4 eV (vs. pure anatase that showed the expected 3.2 eV optical gap, Figure S4 B in the Supporting Information). The magnitude of the visible response considerably increased with an increasing precursor amount up to the optimum loading of 15 mg (Figure S4 A in the Supporting Information). The enhancement of IPCE for g-C_3N_4/TiNTs samples could be ascribed to the wider absorption spectrum region and the improved charge separation and transportation efficiency by the nanojunctions between the TiO_2 nanotubes and g-C_3N_4 polymer. In the following study, 15 mg melamine was used for preparing g-C_3N_4/TiNTs samples. However, a drop of IPCE was observed when 20 mg precursors were employed, which was likely due to the blocking of nanotube entrance by a thick g-C_3N_4 layer (as illustrated in Figure S2 in the Supporting Information).

Figure 3 A shows the photoelectrochemical properties of g-C_3N_4/TiNTs before and after Pt grafting. Since Pt-decorated anatase TiO_2 nanostructures (such as nanoparticles and nanotubes) have been studied extensively, we used anatase TiNTs before and after Pt decoration (Pt-TiNT) for reference. In the visible range, the bare TiNTs exhibited only a very low response. Pt-decorated g-C_3N_4/TiNTs and TiNTs samples exhibited a slightly enhanced IPCE in the visible light range, which was likely due to the increased separation of photogenerated electrons and holes at the heterojunctions. It is noteworthy that the Pt loading on the TiNTs or g-C_3N_4/TiNTs led to an obviously decreased UV response compared with the bare TiNTs and g-C_3N_4/TiNTs. This is due to the "shading" effects of C_3N_4. C_3N_4 also absorbs in the UV range, and less UV light reaches the underlying TiO_2. Figure 3 C shows results for the photoelectro-

chemical water splitting performance under simulated sunlight AM 1.5 (100 mW cm^{-2}) with a UV-cutoff filter ($\lambda < 400$ nm) in 0.1 M Na_2SO_4. From the photocurrent transient vs. potential curves, it is apparent that the Pt-decorated g-C_3N_4/TiNTs sample exhibits the highest photocurrents over the entire range. For comparison, a bare TiNTs layer loaded with a similar density of Pt nanoparticles was used. It was evident that the Pt/g-C_3N_4/TiNTs heterojunctions exhibited a very good photocatalytic performance at open-circuit condition under visible light. Moreover, the photocatalytic activity for bias-free H_2 production was further investigated in water (containing 20% ethanol as a hole capture agent) under AM 1.5 illumination conditions. Gas chromatography (GC) analyses (Figure 3 D) revealed an H_2 production rate of 0.78 µL h^{-1} cm^{-2} for g-C_3N_4/TiNTs. These tubes, after grafting with Pt nanoparticles, showed an increase of H_2 production rate (15.62 µL h^{-1} cm^{-2}), which was almost a 20-fold H_2 production rate of g-C_3N_4/TiNTs, and a 98-fold H_2 production rate of TiNTs (0.16 µL h^{-1} cm^{-2}).

In conclusion, g-C_3N_4-loaded TiNTs were successfully fabricated. The as-prepared g-C_3N_4/TiNTs exhibited a clearly higher photoelectrochemical activity under visible light conditions. Even more, the Pt-decorated g-C_3N_4/TiNTs showed significantly enhanced photoelectrochemical water splitting activity and had a high potential for energy conversion. Obviously, the g-C_3N_4/TiNTs nanocomposite showed considerable photocatalytic activity in the visible-light range and excellent stability. Moreover, this study provides a simple and fast approach to grafting g-C_3N_4 on 3D nanoporous/nanotubular structures, which then provides a platform with a considerable photocatalytic performance under visible light.

Experimental Section

Preparation of TiO_2 nanotube arrays: Ti foils (0.1 mm thickness, 99.6% purity, Advent) were first degreased by sonication in acetone, EtOH, and deionized H_2O (DI), and then dried in a nitrogen stream. Self-organized TiO_2 nanotube layers with approximately 1.5 µm thickness were grown in glycerol (50 vol %)-H_2O electrolyte containing 0.27 M NH_4F at 30 V for 4 h.[43] The layers were annealed in air at 550 °C for 1 h.

Decoration of g-C_3N_4 layer: Deposition of g-C_3N_4 onto the TiNTs was performed by a chemical vapor deposition (CVD) approach by using melamine as a precursor.[44] Briefly, melamine (5.0–20.0 mg) was added in a cleaned alumina crucible with a cover, and the TiNTs was placed (top-down) several centimeters above the melamine powders, and then the crucible was heated at 550 °C for 3 h in a tube furnace. After the process, the g-C_3N_4 polymer was successfully deposited onto the TiO_2 nanotubes, while some g-C_3N_4 powder was also obtained in the crucible.

Decoration with Pt nanoparticles: Pt-decorated g-C_3N_4/TiNTs samples were prepared by sputtering Pt nanoparticles via a plasma sputter equipment (EM SCD500, Leica, Wetzlar, Germany) at 15 mA at 1 bar of Ar condition (at a normal loading of 1 nm).

Apparatus: The morphologies of the g-C_3N_4/TiNTs were characterized using a field-emission SEM (Hitachi FE-SEM S4800, Tokyo, Japan). X-ray diffraction (XRD) patterns were acquired on an X'Pert X-ray diffraction spectrometer (Philips, Andover, MA, USA) with a Cu Kα X-ray source. The composition of the layers was analyzed

using an X-ray photoelectron spectrometer (XPS, PHI 5600, Physical Electronics, Chanhassen, MN, USA) using Al Kα radiation at 13 kV as excitation source with a takeoff angle of 45° for the emitted photoelectrons. All the peaks are shifted based on a standard of C 1s at 284.8 eV. A three-electrode configuration containing the TiNTs as photoanode, Pt foil as cathode, and Ag/AgCl (3 M KCl) as reference electrode was employed for all photoelectrochemical experiments. Photocurrent measurements were performed with a setup consisting of a 150 W Xenon lamp as the light source. Photocurrent spectra were acquired in 10 nm steps in a range of 300–700 nm in an aqueous solution of 0.1 M Na_2SO_4 at an applied bias of +0.5 V. The value of photocurrent density was measured as a difference between current densities acquired under irradiation and in the dark, and then IPCE was calculated from the measured photocurrent densities. The water-splitting performance experiments were carried out by applying an external bias to the cell with a scan rate of 1 mV s^{-1} at rt. The light source was a 300 W Xenon lamp (100 mW cm^{-2}) with a cutoff filter $\lambda < 400$ nm. The photocatalytic H_2 production tests were carried under simulated AM 1.5 illumination provided by a solar simulator (300 W Xe with optical filter, Solarlight, Glenside, PA, USA).

Acknowledgements

[1] A. Fujishima, K. Honda, *Nature* **1972**, *238*, 37–38.
[2] X. Chen, S. Shen, L. Guo, S. S. Mao, *Chem. Rev.* **2010**, *110*, 6503–6570.
[3] R. Asahi, T. Morikawa, T. Ohwaki, K. Aoki, Y. Taga, *Science* **2001**, *293*, 269–271.
[4] I. Paramasivam, H. Jha, N. Liu, P. Schmuki, *Small* **2012**, *8*, 3073–3103.
[5] Y. Y. Song, F. Schmidt-Stein, S. Bauer, P. Schmuki, *J. Am. Chem. Soc.* **2009**, *131*, 4230–4232.
[6] A. L. Linsebigler, G. Lu, J. T. Yates, *Chem. Rev.* **1995**, *95*, 735–758.
[7] M. R. Hoffmann, S. T. Martin, W. Choi, D. W. Bahnemann, *Chem. Rev.* **1995**, *95*, 69–96.
[8] X. M. Zhou, N. T. Nguyen, S. Özkana, P. Schmuki, *Electrochem. Commun.* **2014**, *46*, 157–162.
[9] K. Lee, A. Mazare, P. Schmuki, *Chem. Rev.* **2014**, *114*, 9385–9454.
[10] P. Roy, S. Berger, P. Schmuki, *Angew. Chem. Int. Ed.* **2011**, *50*, 2904–2939; *Angew. Chem.* **2011**, *123*, 2956–2995.
[11] J. M. Macak, M. Zlamal, J. Krysa, P. Schmuki, *Small* **2007**, *3*, 300–304.
[12] D. R. Baker, P. V. Kamat, *Adv. Funct. Mater.* **2009**, *19*, 805–811.
[13] M. Yang, D. Kim, H. Jha, K. Lee, J. Paul, P. Schmuki, *Chem. Commun.* **2011**, *47*, 7746–7768.
[14] M. Grätzel, *Nature* **2001**, *414*, 338–344.
[15] W. T. Sun, Y. Yu, H. Y. Pan, X. F. Gao, Q. Chen, L.-M. Peng, *J. Am. Chem. Soc.* **2008**, *130*, 1124–1125.
[16] A. Kongkanand, K. Tvrdy, K. Takechi, M. Kuno, P. V. Kamat, *J. Am. Chem. Soc.* **2008**, *130*, 4007–4015.
[17] H. Gerischer, M. Luebke, *J. Electroanal. Chem.* **1986**, *204*, 225–227.
[18] R. Plass, S. Pelet, J. Krueger, M. Gratzel, U. Bach, *J. Phys. Chem. B* **2002**, *106*, 7578–7580.
[19] L. Yang, S. Luo, R. Liu, Q. Cai, Y. Xiao, S. Liu, F. Su, L. Wen, *J. Phys. Chem. C* **2010**, *114*, 4783–4789.
[20] J. Lin, J. Chen, X. Chen, R. Zong, M. Zhou, Y. Zhu, *Appl. Catal. B* **2009**, *89*, 425–431.
[21] C. Liu, Y. Teng, R. Liu, S. Luo, Y. Tang, L. Chen, Q. Cai, *Carbon* **2011**, *49*, 5312–5320.
[22] J. Yu, G. Dai, B. Huang, *J. Phys. Chem. C* **2009**, *113*, 16394–16401.
[23] N. K. Shrestha, M. Yang, I. Paramasivam, P. Schmuki, *Semicond. Sci. Technol.* **2011**, *26*, 092002.
[24] R. Beranek, J. M. Macak, M. Gärtner, K. Meyer, P. Schmuki, *Electrochim. Acta* **2009**, *54*, 2640–2646.
[25] A. Thomas, A. Fischer, F. Goettmann, M. Antonietti, J. Muller, R. Schlogl, J. M. Carlsson, *J. Mater. Chem.* **2008**, *18*, 4893–4908.
[26] E. Kroke, M. Schwarz, *Coord. Chem. Rev.* **2004**, *248*, 493–532.
[27] F. Goettmann, A. Fischer, A. Thomas, M. Antonietti, *Angew. Chem. Int. Ed.* **2006**, *45*, 4467–4471; *Angew. Chem.* **2006**, *118*, 4579–4583.
[28] M. Groenewolt, M. Antonietti, *Adv. Mater.* **2005**, *17*, 1789–1792.
[29] Y. J. Zhang, T. Mori, J. H. Ye, M. Antonietti, *J. Am. Chem. Soc.* **2010**, *132*, 6294–6295.
[30] Y. Wang, Y. Di, M. Antonietti, H. Li, X. F. Chen, X. C. Wang, *Chem. Mater.* **2010**, *22*, 5119–5121.
[31] J. Liang, Y. Zheng, J. Chen, J. Liu, D. Hulicova-Jurcakova, M. Jaroniec, S. Z. Qiao, *Angew. Chem.* **2012**, *124*, 3958–3962.
[32] G. Liu, P. Niu, C. H. Sun, S. C. Smith, Z. G. Chen, G. Q. Lu, H. M. Cheng, *J. Am. Chem. Soc.* **2010**, *132*, 11642–11648.
[33] X. C. Wang, K. Maeda, X. F. Chen, K. Takanabe, K. Domen, Y. D. Hou, X. Z. Fu, M. Antonietti, *J. Am. Chem. Soc.* **2009**, *131*, 1680–1681.
[34] Y. J. Zhang, A. Thomas, M. Antonietti, X. C. Wang, *J. Am. Chem. Soc.* **2009**, *131*, 50–51.
[35] G. Z. Liao, S. Chen, X. Quan, H. T. Yu, H. M. Zhao, *J. Mater. Chem.* **2012**, *22*, 2721–2726.
[36] L. Ge, F. Zuo, J. k. Liu, Q. Ma, C. Wang, D. Z. Sun, L. Bartels, P. Y. Feng, *J. Phys. Chem. C* **2012**, *116*, 13708–13714.
[37] S. C. Yan, S. B. Lv, Z. S. Li, Z. G. Zou, *Dalton Trans.* **2010**, *39*, 1488–1491.
[38] H. J. Yan, H. X. Yang, *J. Alloys Compd.* **2011**, *509*, L26–L29.
[39] W. Liu, M. Wang, C. Xu, S. Chen, X. Fu, *J. Mol. Catal. A* **2013**, *368–369*, 9–15.
[40] L. Zhang, D. Jing, X. She, H. Liu, D. Yang, Y. Lu, J. Li, Z. Zheng, L. Guo, *J. Mater. Chem. A* **2014**, *2*, 2071–2078.
[41] A. Vinu, *Adv. Funct. Mater.* **2008**, *18*, 816–827.
[42] J. Zhong, J. J. Deng, B. H. Mao, T. Xie, X. H. Sun, Z. G. Mou, C. H. Hong, P. Yang, S. D. Wang, *Carbon* **2012**, *50*, 335–338.
[43] Y. Y. Song, Q. L. Zhuang, C. Y. Li, H. F. Liu, J. Cao, Z. D. Gao, *Electrochem. Commun.* **2012**, *16*, 44–48.
[44] S. C. Yan, Z. S. Li, Z. G. Zou, *Langmuir* **2009**, *25*, 10397–10401.